Dielectric Permittivity and AC Conductivity Investigation for the New Model Lipid Bilayer Material: $(CH_2)_{10}(NH_3)_2CdCl_4$

Mohga F. Mostafa and Ahmed A. A. Youssef

Physics Department, Faculty of Science, University of Cairo, Giza, Egypt

Reprint requests to Dr. M. F. M.; E-mail: MOHGA@FRCU,EUN.EG

Z. Naturforsch. **56a,** 568–578 (2001); received April 26, 2001

Differential thermal scanning of the new lipid-like bilayer material $(CH_2)_{10}(NH_3)_2CdCl_4$ showed two structural phase transitions, with onset temperatures at $T_2 = (359 \pm 2)$ K and $T_1 = (415 \pm 1)$ K. Permittivity measurements were performed between room temperature and 450 K at 60–100 kHz. A step-like rise in permittivity at T_2, associated with an order-disorder transition, is attributed to chain melting. Two anomalies at (413 ± 1) K and (430 ± 3) K, showing thermal hysteresis of ~8 and 10 K, respectively, indicate first order transitions which are associated with crystalline phase change.

The AC conductivity follows an Arrhenius-type relation with the activation energy ΔE varying with the frequency f according to the relation $\Delta E = \Delta E_0\,[1 - \exp(f_0/f)]^{\alpha}$, where ΔE_0, f_0 and α are 0.95 eV, 52 Hz and 0.11, respectively. The frequency dependent conductivity follows the power law $\sigma = \sigma_{dc} + B\omega^s$, with $0.3 < s < 1.5$ for hopping conduction of hydrogen and/or chloride ions in the high temperature range, and localized hopping and/or orientational motion predominating temperatures lower than 413 K. Variations of B and s with temperature are discussed. PACS No. 76, 77

Key words: Phase Transitions; AC Dielectric Permittivity; Two-dimensional Materials; Lipid Bilayers.

1. Introduction

For the past years we have been interested in the magnetic and electric properties of low dimensional systems [1–5]. Of particular interest are systems having long chains of alkyl- or alkylene-groups, as they provide good model for biologically significant lipid membranes [6–10]. Phospholipid bi-layers were found to undergo two transitions, a pre-melting transition at 35 °C and a main transition at ~ 41 °C. The nature of the pre-melting transitions is not well understood and has been attributed to slight reorientations of the chains [6–11]. The main transition was named "chain melting transition" [8]. Chain melting is defined as rapid diffusion of one or more gauche bonds up and down the hydrocarbon chain. Since lipid layers are inherently liquid systems, it is difficult to study them by solid state techniques. The alkylene-chain complexes provide the basis for systems that combine bi-layer characteristics within a crystalline lattice. The long chain alkylene-diammonium complexes; $(CH_2)_n(NH_3)_2MX_4$ for $n \geq 5$ (M is a divalent transition metal ion and X a halide ion) are known to undergo several structural phase changes, some of which are found near ambient temperature [12, 13]. These phase transitions have been studied by different techniques [12–16]. In such systems the transition metal ion is in a distorted octahedra of halogen ions. These octahedra share corners forming well-characterized two-dimensional perovskite-like sheets. The $[(CH_2)_n(NH_3)_2]^+$ groups separate these metal halide layers, and for large values of n, a quasi-two dimensional system is obtained.

Phase changes in the materials are a result of an interplay between the planar system of corner-sharing metal-halide octahedra and the motion of the alkylene chains $[(CH_2)_n]$ located between the octahedral planes. For chains with $n \geq 4$, structural rearrangement, due to conformational changes of the chain play an important role [12–14]. Structure determination of $(CH_2)_n(NH_3)_2MX_4$, B = Mn, Cd, ... showed that these materials have essentially the same structural features [12]. The compound with $n = 2$ shows no structural phase transitions up to the decomposition temperature. The compounds with $n > 2$ and M = Cd, Mn, Fe or Cu [13–16] show first and second order phase transformation, as listed in Table 1.

It is to be noted that the room temperature phase of odd carbon number compounds is orthorhombic, whereas that of even carbon number compounds is monoclinic [12–15]. This even-odd structure dependence seems to affect the static dielectric constant, where ε' drops on heating through the transition for materials containing even number C-atoms [13]. Permanent dipoles exist for odd carbon number but does not exist in even carbon number compounds. This is because of the center of inversion in the middle of the chain.

0932-0784 / 01 / 0800-0568 $ 06.00 © Verlag der Zeitschrift für Naturforschung, Tübingen · www.znaturforsch.com

Table 1. List of the transition temperatures of $(CH_3)_n(NH_3)_2BX_4$, B = MN and Cd, X = Cl.

Compound	T_{tr} (K)	Order	Reference
$(CH_2)_3(NH_3)_2CdCl_4$	375	2^{nd}	[12, 14]
$(CH_2)_3(NH_3)_2MnCl_4$	336	1^{st}	[12, 14]
$(CH_2)_4(NH_3)_2MnCl_4$	382	2^{nd}	[13]
$(CH_2)_4(NH_3)_2CdCl_4$	341	1^{st}	[14]
$(CH_2)_5(NH_3)_2CdCl_4$	338	2^{nd}	[14]
$(CH_2)_5(NH_3)_2CdCl_4$	412	–	[13, 14]
$(CH_2)_4(NH_3)_2PbCl_4$	323.8	1^{st}	[15]
$(CH_2)_3(NH_3)_2FeCl_4$	230	2^{nd}	[16]
$(CH_2)_6(NH_3)_2FeCl_4$	245	2^{nd}	[16]

The aim of the present work is to characterize the structural phase transitions and to study the frequency and temperature dependence of the dielectric permittivity and ac conductivity for the (decanediammonium) $CdCl_4$, named C10Cd.

2. Experimental

2.1. Samples

The compound was prepared by mixing equimolar ratios of decanediammonium dichloride, $(CH_2)_{10}(NH_3)_2Cl_2$ and $CdCl_2$. $2H_2O$ in acidified alcoholic solution. The mixture was kept at 80 C for two hours, then cooled gradually to room temperature. A cream colored material precipitates out. The material was recrystallized from a mixture of alcohol and ether, and then dried under vacuum. The chemical analysis was carried out at the microanalysis unit at the University of Cairo. It showed that the compound has the correct chemical formula. The analysis results are listed in Table 2.

2.2. Infrared Spectroscopy

The IR spectra between 4000 cm^{-1} and 100 cm^{-1} were obtained on an FTIR 5000 spectrometer.

2.3. Thermal Analysis

Differential thermal analysis measurements were performed on a Shimadzu (50)-differential scanning analyzer (DSC) with a scanning speed of 5 °C/min. The data were calibrated with the melting transition of Indium at 157 °C.

2.4. Dielectric Measurements

The complex dielectric permittivity ε^* in the frequency range 5.0 Hz–100.0 kHz was measured using a computer controlled lock-In amplifier type PAR 5207. The temperature was measured using a copper constantan thermocouple. The samples are in the form of pellets of 8 mm in diameter and 1.0 mm thick. The surfaces were coated with silver paste to ensure good electrical contact. The measuring technique and precautions to avoid stray capacitance are discussed in [17].

3. Results and Discussion

3.1. Infrared

The IR absorption spectrum of C10Cd obtained in the range 200–4000 cm^{-1} is shown in Fig. 1. Table 3 lists observed absorption peaks and their assignment. The most characteristics bands in the infrared are those associated with the CH_2 rocking motions, which are usually strong, and the much weaker CH_2 waggings, which are not always observable. The bands at 610–730 cm^{-1} are assigned to the CH_2 rocking fundamental mode $\delta r(CH_2)$. The CH_2 wagging modes are found at 1150–1400 cm^{-1} for the crys-

Table 3. Absorption bands and their assignment.

Wavenumber (cm^{-1}) for Cd	Attributed to
218, 259.7	M-Cl layer mode
405	M-Cl layer mode
728	$\delta r(CH_2)$.
1405	CH_2 wagging/$(NH_3)^+$/C–H str.
1468–1500	N–H def
1624	N–H def
2851	N–H...Cl
2935	C–H str.
3121, 3146	C–H str. / $(NH_4)^+$ (vs)
3382, 3405, 3428	C–H str.

Table 2. Results of chemical analysis for C10Cd.

Material	C%		H		N		Cl		Metal	
	Calc	fnd	Calc	fnd	Calc	fnd	Calc	fnd	Calc	fnd
$(CH_2)_{10}(NH_3)_2CdCl_4$	35.74	35.25	7.45	6.7	6.95	6.8	35.24	34.1	14.46	14.38

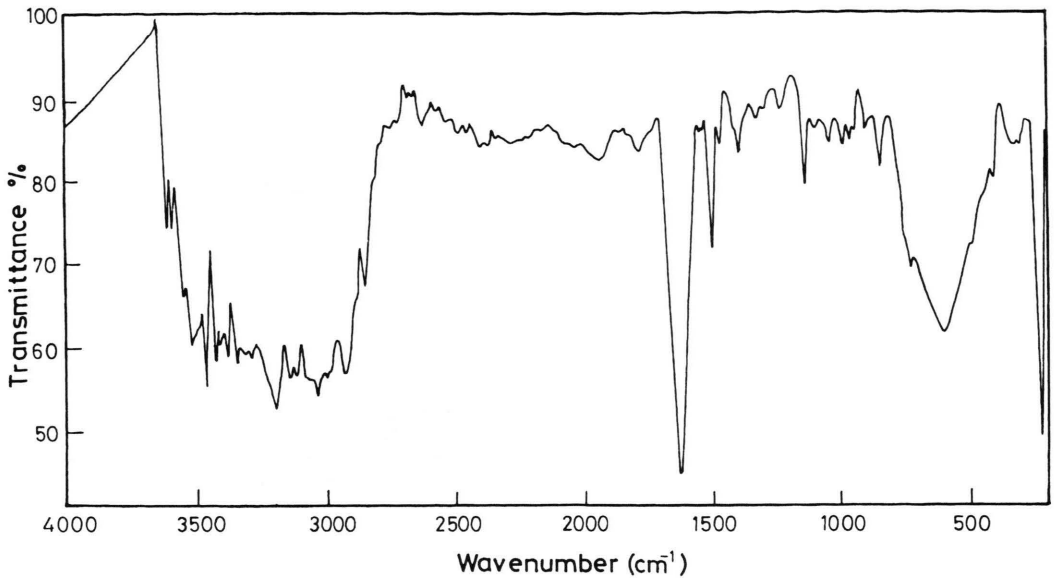

Fig. 1. The IR absorption spectrum of $(CH_2)_{10}(NH_3)_2CdCl_4$.

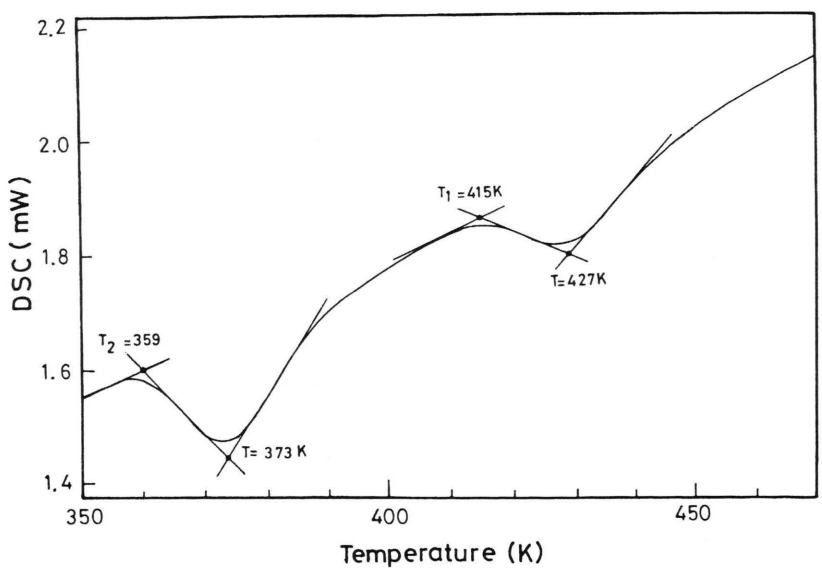

Fig. 2. Differential scanning thermograph of $(CH_2)_{10}(NH_3)_2CdCl_4$ between room temperature and 470 K.

talline *n*-paraffins. These modes are mixed with the $(NH_3)^+$ modes. The coupling with $(NH_3)^+$ may be the reason for the strong enhancement of the intensity of the CH_2 wagging modes compared to the corresponding ones in the case of *n*-alkanes. The bands at 1400–1500 cm^{-1} belong probably to the (NH_3) symmetric deformation mode. The strong bands at 1620 cm^{-1} are assigned to $\delta_{as}(NH_3)$. The bands in the range 400–200 cm^{-1} are typical for M–Cl vibrations [18]. The data of Table 2 are in good agreement with previously published ones on similar compounds [15, 18]. They confirm the presence of the M–Cl layer and, together with the chemical analysis, confirm the formation of the desired materials.

3.2. Differential Scanning Calorimetry (DSC)

The DSC thermograph of the C10Cd powdered sample obtained during heating is shown in Figure 2. Two endo-

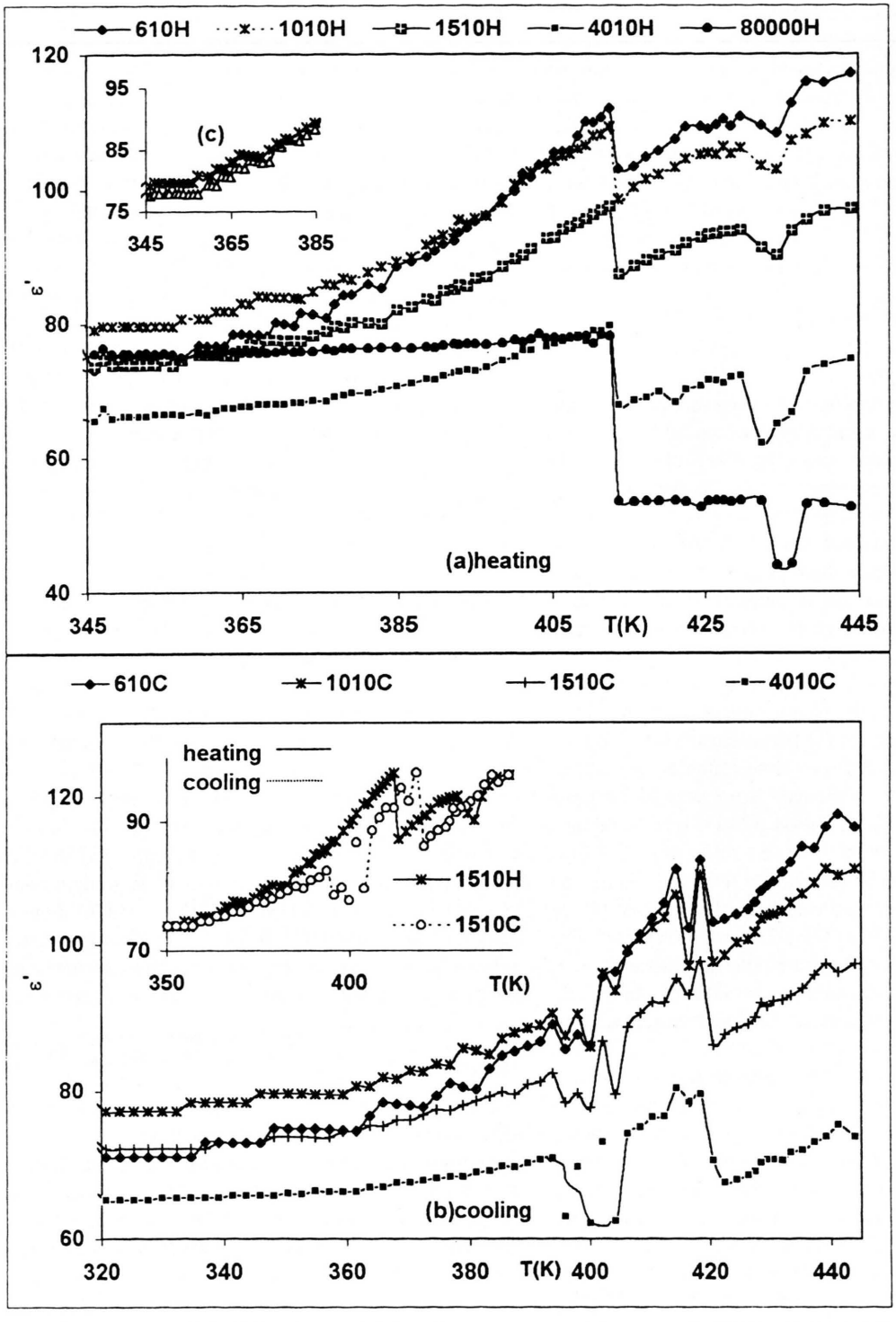

Fig. 3. The real part of the dielectric permittivity (ε') as a function of temperature for $(CH_2)_{10}(NH_3)_2CdCl_4$ at different frequencies. (a) heating up the virgin sample. (b) cooling.

thermic peaks with onset temperatures of $T_1 = (415 \pm 3)$ K and $T_2 = (359 \pm 2)$ K are observed. Both transitions posses high enthalpies, corresponding to entropies of $\Delta S_1 \simeq 7$ and $\Delta S_2 \simeq 14.5$ J/mole-deg, respectively. The high temperature endothermic peak is very broad and has a long temperature tail. It is possible that is comprises two peaks. Although the scan was carried out at the lowest possible rate available, it was not possible to get a better resolution of this peak. The transition temperatures, enthalpies, and entropies obtained from the DSC results are listed in Table 4.

3.3. Permittivity

The temperature dependence of the real part ε' of the complex dielectric permittivity between 60 Hz and 100 kHz in the temperature range 350–450 K obtained while heating and cooling is shown in Figs. 3a and 3b, respectively. Figure 3a shows a gradual rise of (ε') with increasing temperature, which is frequency dependent up to $T_1 =$ 413 K, where a sudden sharp drop in the permittivity is observed. Further increase in temperature shows another drop in permittivity, however lesser in magnitude and sharpness at $T_1' \sim 430$ K. A closer look at the data near the transition temperature $T_2 = 360$ K, shows a step like increase in the permittivity of magnitude ~ 8 units. This is depicted in the insert (c) for frequencies 600 Hz and 2.0 kHz. Lower frequencies show large scattering in this temperature range, and the anomaly is not seen for frequencies higher than 6.0 kHz. This step like rise in the permittivity is ascribed to rotational-type transitions [3, 20]. Figure 3b shows a similar behavior to that obtained for the heating run, however it reflects thermal hysteresis. This is seen as abrupt changes at (420 ± 2) K and (405 ± 1) K. The step-like change noted at T_2 during the heating run is shifted by ~ 4 K to the lower temperature side and can only be seen at the lowest frequencies. The shift in temperature confirms the first order nature of the transition. Usually a large enthalpy is found to be associated with order-disorder transitions. Hence it is possible to relate the step like anomaly at T_2 to an order-disorder transition associated with rotational motions which is found to be accompanied by a large entropy change ($\Delta S = 14.5$ J/mole-deg). This is very likely related to a chain melting transition. This involves cooperative conformational changes of the alkylene chains. Here one deals with order-disorder transitions among the three relative orientations alternate N–C or C–C bonds can take on: the trans-(t), the gauche plus (g) and the gauche minus (g-) configurations, which all differ by ~120° from each other, forming a special sequence of trans-gauche configurations: gtg-, gtttg-. These groups are dynamically disordered, camping the "trans"-"gauche" transitions in the high temperature phase. By proton NMR data this is found to be connected with the melting of the $-CH_2$ groups [20]. Hence, the conformational transitions and reorientation resulting from this chain melting is associated with the order-disorder transition at $T \sim 360$ K. Recent DSC measurements in our laboratory of $((CH_2)_{12}(NH_3)_2)CuCl_4$ have shown a chain melting transition in the temperature range 330 – 360 K with a similar permittivity behavior to that obtained here [21]. The large sharp drop at $T_1 = 413$ K, followed by another drop at $T_1' = 430$ K, is very likely associated with a drastic rearrangement of the domain structure, which is expected to cause changes in the unit cell dimensions. This is supported by the first order nature of the phase transition as is evidenced from our hysteresis results seen in the insert of Fig. 3b. This shows the heating and cooling results obtained at frequency of 1.0 kHz. There is a significant thermal hysteresis at both transition temperatures with $\Delta T =$ 8 K and 10 K for the T_1 and T_1' respectively. It is likely that two structural phase changes are associated with the reorientation of the dipoles. At this point it is worth mentioning that the entropy value obtained for this transitions (ΔS ~ 7 J/mole-K) supports the occurrence of a structural phase transition. Since there are four consecutive –C–N atoms involved in a torsion angle in the diammonium chain $(CH_2)_{10}(NH_3)_2$, there are eight independent possibilities to form trans- or gauche configurations. There are two limiting values for ΔS: the first is $\Delta S = R$, due to a free rotation around two axes, the second is $\Delta S = R \ln 2 = 0.69\,R$ due to orientation of the R–C–C–R group among two equivalent sites. Our DSC results ($T = 413$ K) showed $\Delta S = 7.3$ J/mole-deg,which lies between these two limiting values. Hence we can safely assume that the chains are completely disordered in the high temperature phase.

3.4. Relaxation

The conductivity relaxation model, in which the dielectric modulus is defined as $M^*(\omega) = 1/\varepsilon^*(\omega)$, may be used to get information about the relaxation mechanism in case there is no well-defined dielectric loss peak [22]. $M^* - \ln(\omega)$ plots at different temperatures are shown in Figs. 4a, b for heating and cooling runs, respectively. As the frequency increases, $M'(\omega)$ increases to a maximum asymptotic value defined as M_∞. The spectra of $M''(\omega)$ show an asymmetric peak approximately centered in the dispersion region of $M'(\omega)$. These plots show features of ionic conduction, namely the S shaped dispersion in M' and a peak

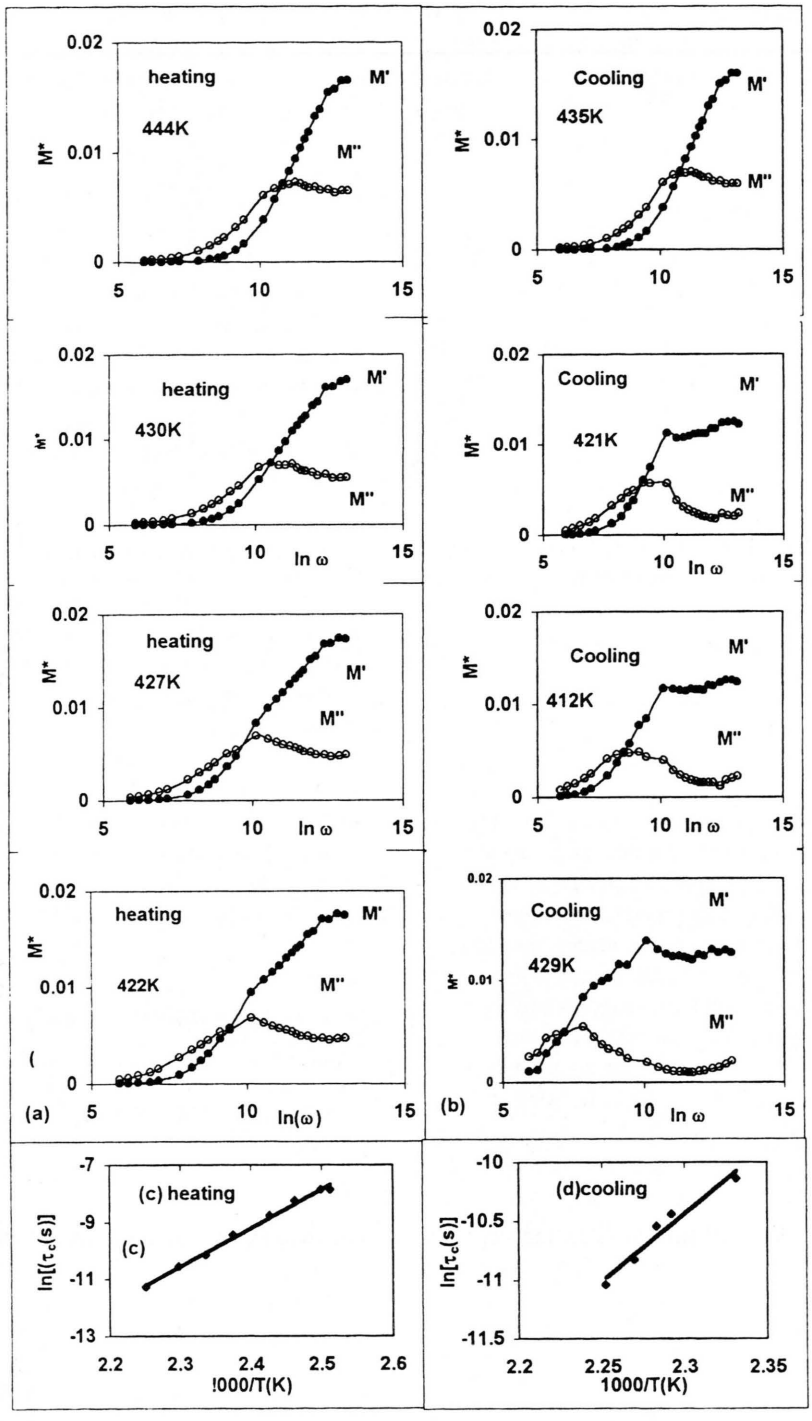

Fig. 4. M^* vs. ln ω at various temperatures: (a) heating; (b) cooling; (c) ln τ_c vs. 1000/T for heating; (d) ln τ_c vs. 1000/T for cooling.

in M'' The relaxation peaks are found to shift towards higher frequencies as temperature increases. The frequency ω_c at which the maximum of M'' (M''_{max}) occurs, defines the conductivity relaxation time τ_c as given by $\omega_c \tau_c = 1$. The variation of the maxima were fitted to (1).

$$\tau_c = \tau_0 \exp(-\Delta W_r/kT), \quad (1)$$

where W_r is the activation energy for the relaxation process and τ_0 is the high temperature limit of the relaxation time. Plots of $\ln(\tau)$ vs. $1000/T$, as shown in Figs. 4c, d, yield $\tau_0 = 8.6 \times 10^{-19}$ s and 7.9×10^{-17} s, and $\Delta W_r = 1.16$ eV and 0.99 eV for heating and cooling runs, respectively.

3.5. Conductivity

3.5.i. Frequency dependence

The dielectric response of low conductivity materials is usually characterized by the well-known universal dynamic response [23]

$$\sigma(\omega) = \sigma_{dc} + B(T)\,\omega^{s(T)}, \quad (2)$$

where σ_{dc} is the dc (or low frequency) conductivity. The universal exponent s and the pre-exponential factor $B(T)$ are both functions of the temperature and the type of conduction mechanism.

Figures 5a, b show the frequency dependence of the ac conductivity at different temperatures as $\ln(\sigma(\omega))$ vs. $\ln(\omega)$ for heating and cooling runs, respectively. Extrapolation of the plateau value of the conductivity gives σ_{dc} at various temperatures. The plot of the values obtained for $\sigma_{dc}(T)$ using the Arrhenius type relation, $\sigma(T) = \sigma_0 \exp(-\Delta E/kT)$ shows four different temperature regions which correspond to the phase (I), (II), (III), and (IV) as shown in Figure 6a. Values of the activation energies as well as the pre-exponential factor (σ_0) are listed in Table 5 for phases the (I), (II) and (III). No results were obtainable for the region of phase (IV) due to the increased scattering at low frequencies, owing to the high resistance of the material. The activation energies differ slightly for the different phases, with the high temperature phase (I) having the lower ΔE values.

Fitting the frequency dependent conductivity after subtracting the dc conductivity yields values of s and $\ln(B)$ shown as function of temperature in Figs. 5c, d for heating and cooling, respectively. Values of $0 < s < 1$ dominate at low frequencies and are found to correspond to a translational hopping motion, whereas values of $1 < s < 2$ dominate at high frequencies and corresponds to well localized hopping and/or reorientational motion [3, 24]. The exponent s decreases linearly with temperature in phases (I) and (III), varying between 1.5–0.8 for phase (III), and 0.56–0.3 for phase (I). Scattering values of s are obtained in the temperature region $T_1 - T_1'$ and near the transition T_2, for the heating and cooling runs. Reorientational motion and or localized hopping are found to be associated with s values in the range of 2-1, while for translational hopping conduction, values varying between 1–0.4 [3, 24] are expected. Hence it is possible to suggest that for $T < 400$ K localized hopping and/or reorientational motion is the main mechanism of conduction. At $T > T_1'$, translational hopping of hydrogen and/or chloride ions are the major contributors to the conduction mechanism. The pre-exponential factors $\ln B_1$ and $\ln B_2$ are linearly dependent on the temperature except at the transition ranges, where anomalous behavior prevails.

3.5.ii. Temperature dependence of σac

Figures 6b, c show logarithmic plots of the conductivity as function of the reciprocal temperature at selected frequencies for heating and cooling, respectively. The conductivity is thermally activated following the Arrhenius relation. The least squares fit to the Arrhenius relation results in an activation energy that is frequency dependent, as shown in Fig. 6d for the heating runs. Similar results are obtained for data collected while cooling. The values of the activation energies in all regions lie within the range of ionic conduction. The dependence of the activation energy on the frequency in the range 360–411 K for heat-

Table 4. Transition temperatures, enthalpies and entropies as obtained from DSC.

Transition temperature	T_1 (K)	T_2 (K)
T (on set) heating	413	360
T (peak) heating	427	373
ΔH J/mole	3068	5428
ΔS J/mole-deg	7.4	14.5

Table 5. Activation energies for dc conductivity.

Phase	Temperature	Heating	Cooling
(III)	$360 < T < 411$ K	$\Delta E = 0.89$ eV $\sigma_0 = 1.5 \times 10^8$	$\Delta E = 0.83$ eV $\sigma_0 = 1.4 \times 10^7$
(II) cooling	$406 < T < 420$ K^C	$\Delta E = 0.945$ eV	$\Delta E = 0.933$ eV
(II) heating	$414 < T < 427$ K^H	$\sigma_0 = 4.3 \times 10^8$	$\sigma_0 = 3.3 \times 10^7$
(I)	$430 < T < 441$ K	$\Delta E = 0.95$ eV $\sigma_0 = 8.03 \times 10^8$	$\Delta E = 0.907$ eV $\sigma_0 = 1.7 \times 10^8$

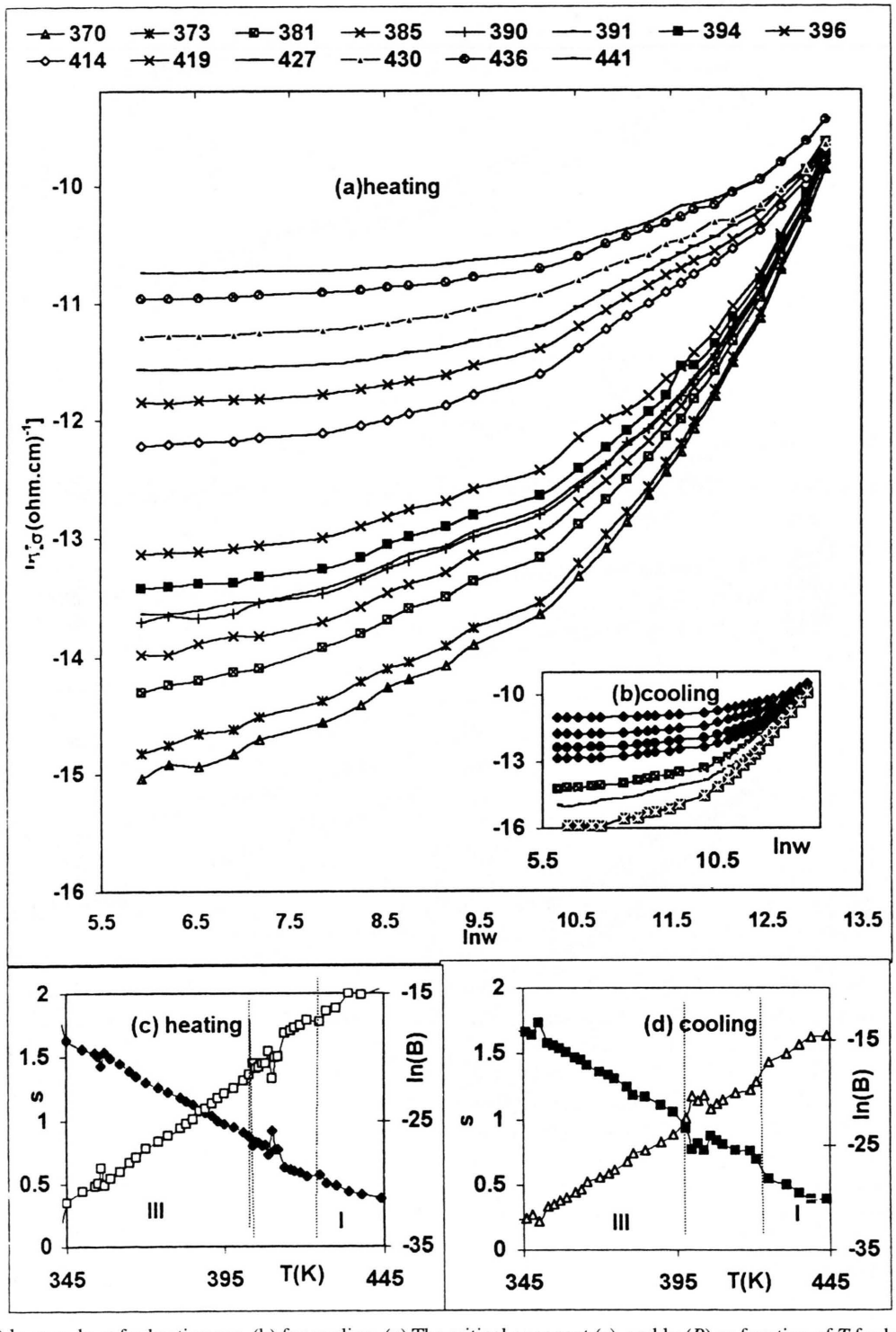

Fig. 5. (a) ln σ vs. ln ω for heating run, (b) for cooling. (c) The critical exponent (s), and ln (B) as function of T for heating. (d) The critical exponent (s), and ln (B) as function of T for cooling.

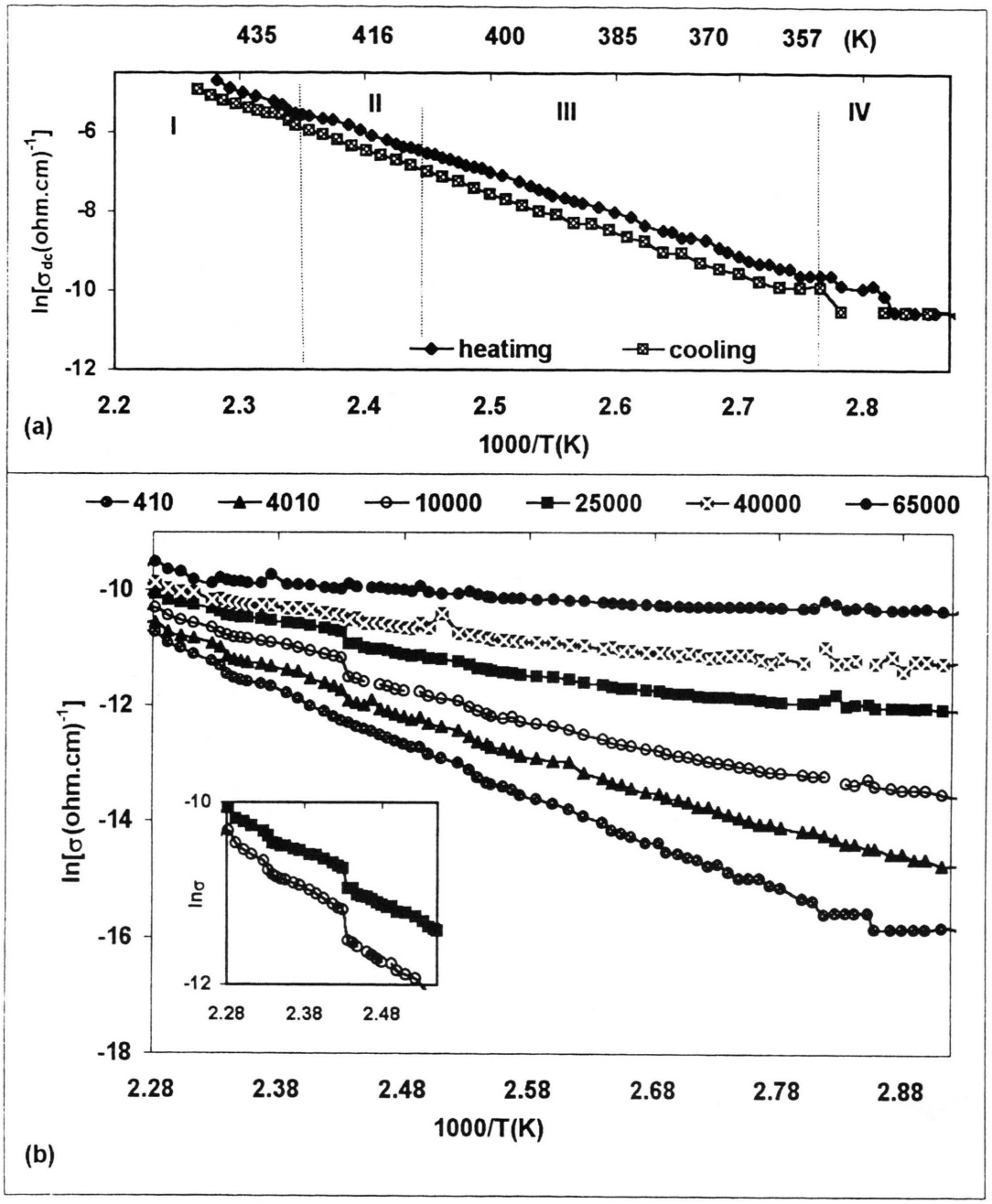

Fig. 6. (a) ln σ_{dc} vs. 1000/T; (b) ln σ_{ac} vs. 1000/T at selected frequencies for heating; (c) ln σ_{ac} vs. 1000/T at selected frequencies for heating; (d) Activation energy vs. frequency in the range 413 K > T > 360 K.

ing, is fitted to (3)

$$\Delta E = \Delta E_0 \, [1 - \exp(-f_0/f)]^{\alpha}, \tag{3}$$

This yields values of ΔE_0, f_0 and α of 0.95 eV, 52 Hz and 0.11, respectively.

Conclusion

DSC, dielectric and conductivity measurements confirm the conformational and rotational motion of $[(CH_2)_{10}(NH_3)_2]^+$ as well as translational hopping of hy-

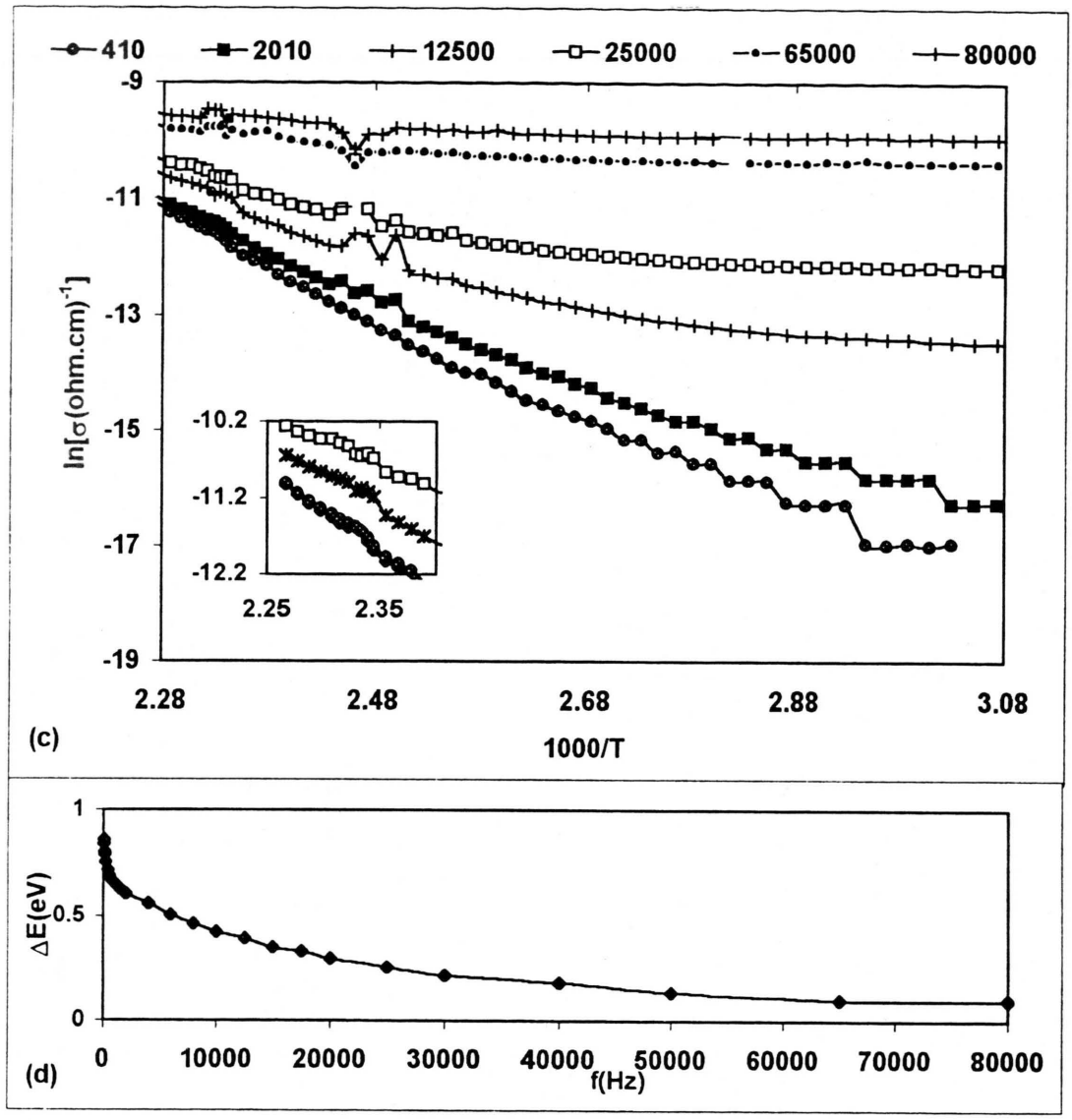

Fig. 6. (c) and (d).

drogen and/or chloride ions in the temperature range studied. Previous studies on similar materials in our laboratory and elsewhere have indicated that the dielectric constant above a transition temperature is usually higher than below it [4, 25] which is found to be the case for the T_2 transition. This is because the main contribution to the dielectric constant arises from the mobility of the anion and cation moieties. Thus the dielectric constant below the phase transition should be lower than that above it, because at lower temperatures the cation and anion are less mobile.

At T_1 the opposite is observed, showing a sudden drop and a lowering of the permittivity above the transition temperature. Hence we suggest that a subtle crystalline transition from the room temperature monoclinic phase to another, probably orthorhombic phase takes place, where in the new phase the anions and cations are less mobile. Further increase in temperature is associated with another crystalline phase change (at T_1') to the parent tetragonal phase where the mobility starts to increase with further increase in temperature. The C10Cd material undergoes 3

phase transitions at T_1, T_1' and T_2. An order-disorder phase transformation occurs at T_2, accompanied by a large entropy change, which is ascribed to chain melting. This involves gauch-trans orientation of the alkylene-diammonium chain. The higher transition temperature may involve subtle crystalline transitions, where a change in the orientation of the alkylene-diammonium occurs. The transition from the room temperature monoclinic structure (Phase IV) to the parent tetragonal (phase I) occurs through another phase, probably orthorhombic. These crystalline transitions are found to be associated with a drop in permittivity and may be associated with a change in the chain alignment from a tilted position to a position perpendicular to the octahedral anion [14, 15, 19]. Such transitions are very common in long chain alkylene-diammonium complexes.

[1] M. F. Mostafa, M. A. Semary, and M. M. Abdel-Kadar, Physica **112B,** 197 (1982).
[2] M. F. Mostafa, M. Abdel-Kader, S. Arafat, and E. Kandeel, Phys. Scrip. **43,** 627 (1991).
[3] M. F. Mostafa and A. S. Atallah, Phys. Lett. **A264,** 242 (1999).
[4] M. F. Mostafa and S. S. Arafat, Z. Naturforsch. **55a,** 595 (2000).
[5] M. F. Mostafa and S. Montasser, Z. Naturforsch. **55a,** 945 (2000).
[6] R. E. Jacobs, B. S. Hudson, and H. C. Anderson, Biochem. **16,** 4349 (1977).
[7] J. L. Ranck, Mol. Biol. **85,** 249 (1974).
[8] L. A. Sklar, B. S. Hudson, and R. D. Simori, Proc. Natl. Acad. Sci USA **72,** 1629 (1975)
[9] M. Janisk, D. Small, and G. Shipley, Biochem. **15,** 4576 (1976).
[10] R. Rand, D. Chapman, and K. Larson, Biophys. J. **15,** 1117 (1975).
[11] B. P. Gaber, P. Yager, and W. L. Petiocolas, Biophys. J. **24,** 677 (1978) and references therein.
[12] K. Tichy, J. Benes, and H. Arend, Acta. Cryst. **B36,** 1355. (1980).
[13] A. Fouskova, Ferroelectrics **25,** 451 (1980)
[14] R. Kind, S. Plesko, P. Gunter, J. Roos, and J. Fousek, Phys. Rev. **B23,** 5301 (1981).
[15] S. Kammoun and A. Daoud, Phys. Stat. Sol. **162,** 575 (1997).
[16] M. F. Mostafa, A. S.Atallah, and R. Emrick, J. Appl. Phys. **81,** 4134 (1997).
[17] M. F. Mostafa, M. M. Abdel-Kadar, A. S. Atallah, and M. El-Nimer, Phys. Stat. Sol. **135(a),** 549 (1993).
[18] S. Kaarup and R. Burg, J. Sol. Stat. Chem. **26,** 59 (1978).
[19] C. Courseille, N. Chanh, Th. Maris, A. Daoud, Y. Abed, and M. Laguerre, Phys. Stat. Sol. **143a,** 203 (1994).
[20] A. Levstik, C. Filipic, R. Blinc, H. Arend, and R. Kind, Solid Stat. Comm. **20,** 127 (1976).
[21] M. F. Mostafa and S. Abdel-Hakim, Paper presented at the solid state conference in Hurgada. Egypt (March-2001).
[22] P. B. Macedo, C. T. Moynihan, and R. Bose, Phys. Chem. Glass. **13,** 171 (1972).
[23] A. K. Jonscher, Dielectric Relaxation in Solids, Chelsea Dielectric Press, London 1983.
[24] M. Cutroni, A. Mandanice, A. Piccolo, C. Fanggao, G. A. Saunders, and P. Mustarelli, Phil. Mag. **73,** 349 (1996).
[25] A. J. Wolthius, W. J. Huiskamp, L. J. De Jongh, and R. L. Carlin, Physica **142B,** 301 (1986).